Korean J. Chem. Eng., **30**(1), 221-227 (2013)
DOI: 10.1007/s11814-012-0124-y

Preparation of anodic aluminum oxide (AAO) nano-template on silicon and its application to one-dimensional copper nano-pillar array formation

Lan Shen*, Mubarak Ali*, Zhengbin Gu*, Bonggi Min, Dongwook Kim*, and Chinho Park*,†**

*School of Chemical Engineering, Yeungnam University, 214-1, Dae-dong, Gyeongsan 712-749, Korea
**Center for Research Facilities, Yeungnam University, 214-1, Dae-dong, Gyeongsan 712-749, Korea
(*Received 2 February 2012 • accepted 2 August 2012*)

Abstract−Anodized aluminum oxide (AAO) nanotemplates were prepared using the Al/Si substrates with an aluminum layer thickness of about 300 nm. A two-step anodization process was used to prepare an ordered porous alumina nanotemplate, and the pores of various sizes and depths were constructed electrochemically through anodic oxidation. The optimum morphological structure for large area application was constructed by adjusting the applied potential, temperature, time, and electrolyte concentration. SEM investigations showed that hexagonal-close-packed alumina nano-pore arrays were nicely constructed on Si substrate, having smooth wall morphologies and well-defined diameters. It is also reported that one dimensional copper nanopillars can be fabricated using the tunable nanopore sized AAO/Si template, by controlling the copper deposition process.

Key words: Anodic Aluminum Oxide (AAO), Copper, Self-assembly, Nano-pore, Electrolyte

INTRODUCTION

Self-ordered nano-porous anodic aluminum oxide (AAO) is a versatile platform for applications in the fields of sensing, storage, separation, and the synthesis of one-dimensional nanostructures [1]. In contrast to mesoporous materials formed by the self-assembly of surfactants and block copolymers, AAOs consist of arrays of nanopores with high aspect ratios that may extend several cm^2 [2]. Self-ordered AAOs are obtained by mild anodization (MA) in three major self-ordering regimes with H_2SO_4, $H_2C_2O_4$, and H_3PO_4 solutions as electrolytes under appropriate electrochemical conditions [3-5]. The synthesis and application of nanoporous alumina mask and titania nanotube thin films by anodization was also reported in the literature [6,7]. The MA process, however, requires an anodization time of typically more than two days, and self-ordered pore growth only occurs within narrow process windows. Various attempts have been made to overcome the drawbacks associated with the MA process [8]. A particularly attractive alternative is the hard anodization (HA) of Al substrates typically performed at high anodization voltages (U) ranging from 40-150 V. $H_2C_2O_4$-based HA enables the rapid fabrication of long-range ordered AAOs under self-ordering regimes characterized by inter-pore distances (D_{int}) between 200 and 300 nm, a range that is not accessible by conventional MA. Moreover, $H_2C_2O_4$-HA allows one to circumvent the time-consuming two-step procedure required for MA. Nanopores with diameters (D_p) ranging from 49 to 59 nm and depths (T_p) ranging from 50 to 70 nm can be grown on a time scale of 1 h and, therefore much faster than those formed under MA conditions. Another important advantage of the HA process is the accessibility of AAOs with porosities (portion of the pore openings of the membrane surface) three-times lower than that of MA membranes. Nanoporous materials have also attracted considerable attention for a wide range of applications in catalysis, sensing and bio-detection due to their large surface-to-volume ratios and excellent thermal and electrical conductivity. Several chemical and physical approaches have been proposed to fabricate nano-porous materials and, among them, anodization holds a unique promise to produce bicontinuous nanoporosity with open pores in three dimensions. Recently, a number of nanoporous metals, including gold, nickel, tungsten, platinum, palladium, and copper have been synthesized by chemical or electrochemical processes [9]. Electrochemical self assembly of copper/cuprous oxide layered nanostructures has been reported [10]. One of the most important applications of nanostructured metals is as active substrates of surface enhanced Raman scattering (SERS) for detecting molecules and for investigating the interaction between molecules and metal surfaces [11].

We systematically investigated the formation and characterization of one-dimensional copper in AAO nanopores at various anodizing conditions. In addition to the distinct anodization parameters (electrolyte type, concentration, temperature and applied potential) that influence considerably the porous structure (D_p and D_{int}) and organization of AAO [12], the surface roughness of the initial Al film also plays a crucial role on the onset of pore nucleation [13]. We compared the presence and absence of electropolishing pretreatment step before anodization in the case of AAO fabrication on Si wafer. Finally, one-dimensional copper nanopillar arrays were formed using the AAO developed in this study and characterized.

EXPERIMENTAL

Aluminum foil (99.999%) was used as a test substrate for optimizing the AAO process. A highly pure Al thin film (99.999%, ~300 nm) was deposited on a p-type silicon (Si) substrate (4.5 inch) by radio frequency (RF) sputtering and used as substrates for the preparation of nanotemplates to form one-dimensional Cu arrays. Cupric

†To whom correspondence should be addressed.
E-mail: chpark@ynu.ac.kr

hydroxide (Junsei, 77%), chromium (VI) oxide (Kanto, 96.0%), oxalic acid (99.5-100.2%), sulfuric acid (95.0%), acetone (99.5%), phosphoric acid (85.0%), ethyl alcohol (94.0%), perchloric acid (60.0-62.0%) from Duksan, and copper(III) sulfate pentahydrate (98%) and lactic acid (95%) from Sigma-Aldrich were used as chemicals. All the solvents were used without further purification. Prior to anodization, the templates were washed by deionized (DI) water under the ultrasonic condition. At all steps, the solution was constantly stirred at a settled speed by a magnetic bar. Anodization was carried out in a 1,000 mL jacketed-beaker designed to keep the temperature of the contained solution constant by using a thermostat. All the glassware, needles, and stirring bars were dried overnight and purged with nitrogen to remove H_2O.

1. Pretreatment of Al Foil

Aluminum foil (99.999%) with the thickness of 0.25 mm was cut into pieces with an area of 1 cm×2 cm and kept in nitrogen atmosphere at 400 ºC for 3 h after being washed by DI water, and naturally cooled to room temperature. It was then electropolished in a solution composed of a mixture of perchloric acid and ethanol ($HClO_4 : C_2H_5OH=1 : 4$) at a constant voltage of 20 V for 1 min. Aluminum foil was used to optimize the anodization process investigated in this study.

2. Pre-preparation of Al/Si Substrate

The substrates were <111> oriented p-type silicon wafers with a resistivity of 5 Ω/cm. A thin layer (~300 nm) of Al with a purity of 99.999% was deposited onto the Si wafer using the RF sputtering. The AAO template fabrication on Si wafer was carried out with or without electropolishing step for verification purposes, and no electropolishing pretreatments were performed for AAO templates to deposit the copper nano-pillars. The sequences of the process used in this study are shown in Fig. 1, which includes the Scheme 1 (formation of AAO template) and Scheme 2 (deposition of one-dimensional copper nano-array), and the detailed experimental conditions are given in Table 1.

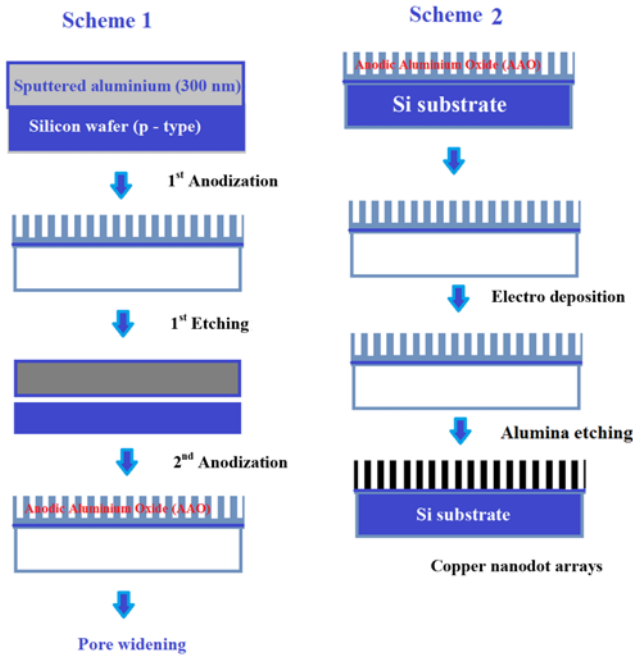

Fig. 1. Schematic diagram of sequence of experimental procedure.

3. Electrodeposition of Nanoporous Cu Nano-pillar Arrays

Following etching and exposure of the metal underlayer as a conduction path for electrodeposition, the pores were ready for filling with copper precursor. The schematic diagram in the present investigation is shown in Fig. 1. The copper nanopillars were formed via DC electrodeposition using a copper counter electrode and a previously published bath composition consisting of 0.6 M copper(II) and 3 M lactate that contained copper(II) sulfate pentahydrate and lactic acid. After a certain amount of 5 M NaOH is added, the solution is stirred overnight with a magnetic stirrer. The stabilized solution is then adjusted to the desired pH of ~10. The electrochemical deposition system employed in this study is a conventional three-electrode system. The counter electrode is a Cu foil while an Ag/AgCl in a 3 M NaCl solution is used as the reference electrode. The electrodeposition is performed under galvanostatic conditions. The voltage is set at 0.1-2 V. The deposited specimen is cleaned with DI water to remove the remaining contaminants. The deposited samples are subsequently immersed in NaOH solution to remove AAO template. The pH of NaOH is varied from 11.0 to 12.0. The duration of immersion is chosen to be 10-30 min. The specimens are finally rinsed with DI water to remove the remaining NaOH.

RESULTS AND DISCUSSION

1. Current-time Characteristics

We recorded the current density as a function of anodization time (I-t curves in Fig. 2) to better understand the anodization process of this study, and the result is explained below. The current density started high in the beginning, decreased as an oxide layer was formed on the surface, and reached a constant level as the pores began to propagate through the aluminum. The current-time behavior during initial anodization process was identical in both freestanding aluminum foils and Al/Si substrates. In the case of Al/Si anodization, an obvious color change occurred resulting from the transparency of the alumina, when the films on the substrates had been nearly completely anodized. At this point, the current also started to change from the steady-state value. In the case of anodization of aluminum sputtered on silicon (p-type) substrates, the current decreased

Table 1. Experimental conditions of multi-step anodization process of AAO/Si template

1st Anodizaiton	1st Etching	2nd Anodization	2nd Etching
Solution: 0.3 M Sulfuric acid	Solution: 1.5 wt% Chromic acid and 6 wt% Phosphoric acid	Solution: 0.3 M Sulfuric acid	Solution: 0.2 M Phosphoric acid
T=15 ºC	T=65 ºC	T=15 ºC	No voltage
Potential=25 V	t=5 min	Potential=25 V	T=25 ºC
t=2 min		t=3 min	t=30 min

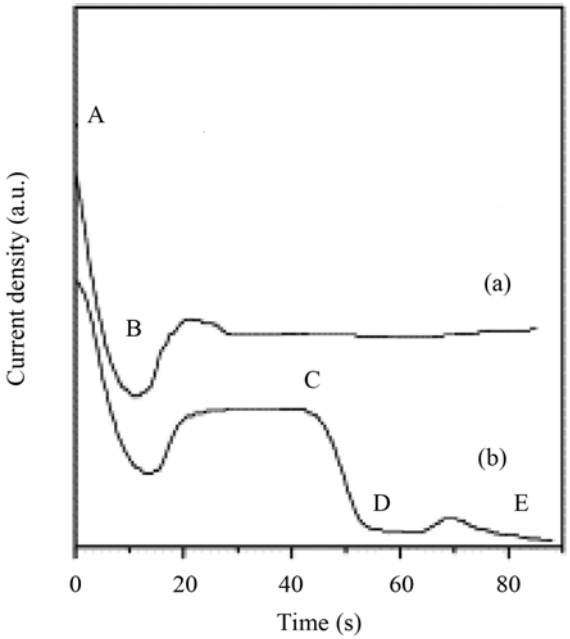

Fig. 2. Current density vs. time (I-t) curve of anodization: (a) Al AAO system (b) Al/Si AAO system.

as the remaining aluminum was consumed. The rate of decrease in current depended strongly on the uniformity of the aluminum film, which in turn depended strongly on the surface roughness of the deposited metal layer. When the aluminum was very smooth with few defects, dark pits were formed on the surface of the film. By characterization with SEM, we determined that the alumina film had been etched away in these pits. The interface between the sputtered aluminum and silicon substrate was not accessible to the anodization solution, as in the case of smooth, uniform films. We stopped the process shortly after the color change when the aluminum films had been completely anodized.

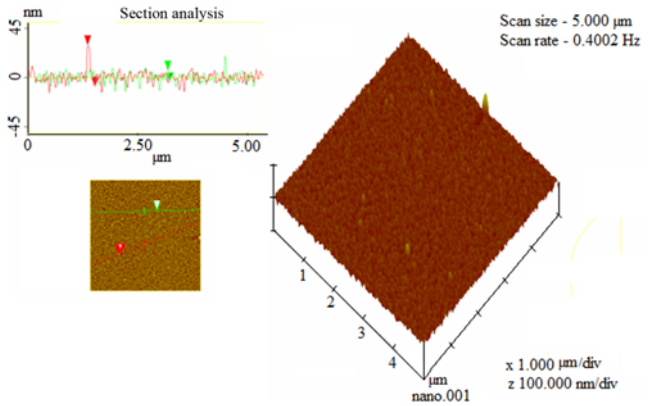

Fig. 3. AFM images of original surface of sputtered aluminum film.

Typical I-t curves of anodization process of this work are shown in Fig. 2. Compared with the I-t curves of bulk Al foil (curve a) and Al/Si substrate (curve b), some new features appear. The A-C range in curve (a) represents the typical I-t behavior during the anodization process of Al film. In the case of Al/Si structure, however, the current is evidently reduced after point C due to the formation of insulating SiO_2 layer.

2. Microscopic Analysis

We investigated the effects of sputtered aluminum on the mor-

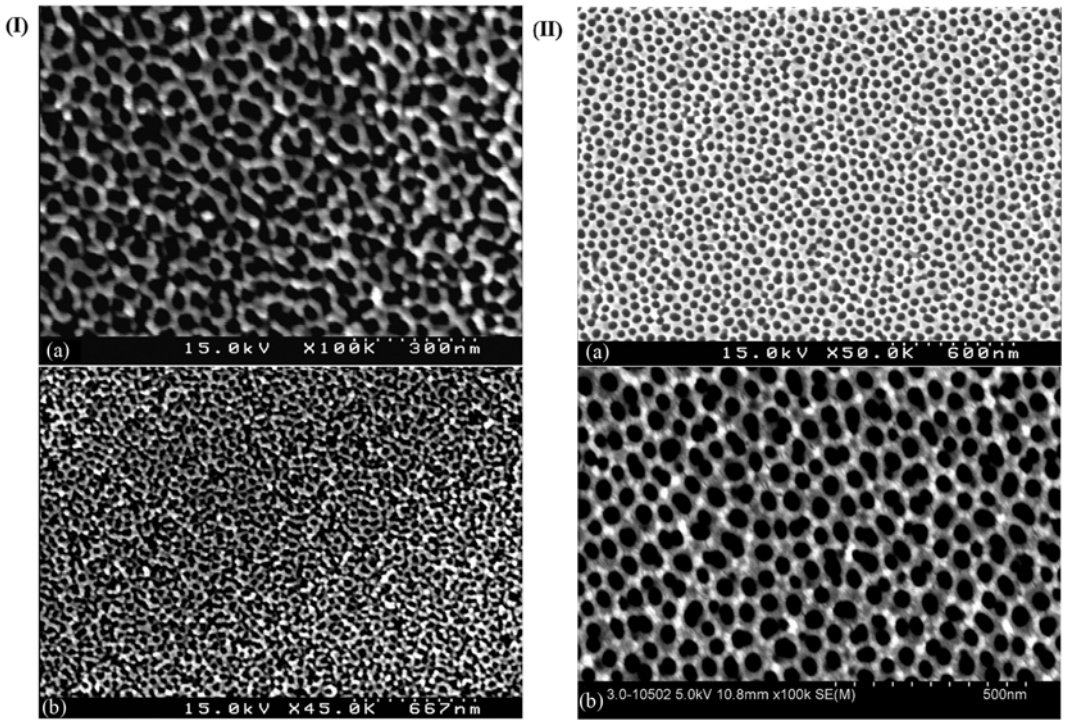

Fig. 4. SEM images of AAO/Si templates with or without pre-electropolishing step.

phology of anodized alumina using atomic force microscopy. Fig. 3 shows top view and 3-D view (AFM) of the aluminum film, and surface roughness of the aluminum was turned out to be quite good (average 5.338 nm). The average surface roughness value was derived from the cross-sectional analysis done by nanoscope image processing software. The morphology of the anodized alumina is strongly related to the original surface roughness of the as-sputtered aluminum. It suggests that ordered and stable anodic oxidation could not take place on the rough surface due to randomly oriented crystal directions of the as-sputtered aluminum. But, in this case, the thickness of the aluminum layer was too thin (300 nm) to undertake any full scale electropolishing process. When we electropolished (the process which is described in the experimental section) the aluminum layer for a very short time (1 min), non-uniform tilted structural nanopores were formed, and the arrangements of pores were also not good.

Anodic dissolution under electropolishing conditions deburrs metal objects due to increased current density on corners and burrs. In our study we tried to fabricate the AAO template with very thin aluminum layer (~300 nm) in order to widen the applicability of the AAO template for thin film devices. If we had conducted the electropolishing step for this thin aluminum film, the film may have been dissolved, which would have resulted in irregular polishing (enough thickness of aluminum film should be on the silicon surface, otherwise the process becomes meaningless for electropolishing of aluminum). For this reason, we obtained low quality AAO templates in our experimentation. So we suggested avoiding the electropolishing step when the AAO template must be reduced with extremely thin aluminum layer.

Fig. 4 shows the influence of electropolishing pretreatment on the nanopore arrangement. Thus, we decided to continue our process without electropolishing pretreatment for Al/Si substrates.

2-1. Effect of Anodizing Parameters on Pore Diameter Variations

Aluminum films were anodized in a 0.2 M sulfuric acid with varying conditions of electrolyte temperature (5 to 20 ºC), time (5 to 20 min) and anodization voltage (25 to 40 V and more than 60 V), taking into account the effect of the pre-anodization treatments. From the microscopic images one can observe that the pore size increases with the increase of voltage, temperature and time, while further increase in time after reaching maximum makes pore size decreased, which can be seen clearly in Fig. 5. In this condition, the cross-sectional view seen in Fig. 6, the result shows uniform, hexagonally ordered (with periodic spacing) pore structures after anodization. Alternatively, ordered, uniform-size pores have been obtained in other work by patterning the initial aluminum film using a mold [14].

2-1-1. Effect of Anodizing Temperature on Pore Diameter

Surface pore density and pore volume increase with temperature (Fig. 5(a)), being the change particularly important when increasing temperature from 10 to 15 ºC [15]. The increase in the electrolyte temperature (Table 2) gives rise to the increase in the number of pores, also increasing their diameters, which results in a porosity increase. The pore sizes were increased from 10 to 40 nm when the temperature was increased from 5 to 20 ºC. The temperature increase leads to an enhancement of the alumina dissolution rate, which results in a decrease of the ohmic resistance and hence of the potential of the process. As previously reported, the potential of the process is directly proportional to the pore size and inversely proportional to the pore density [16-18]. The reaction involved in the anodic oxidation of aluminum is exothermic.

The dissolution of the resulting oxide by the acid electrolyte is

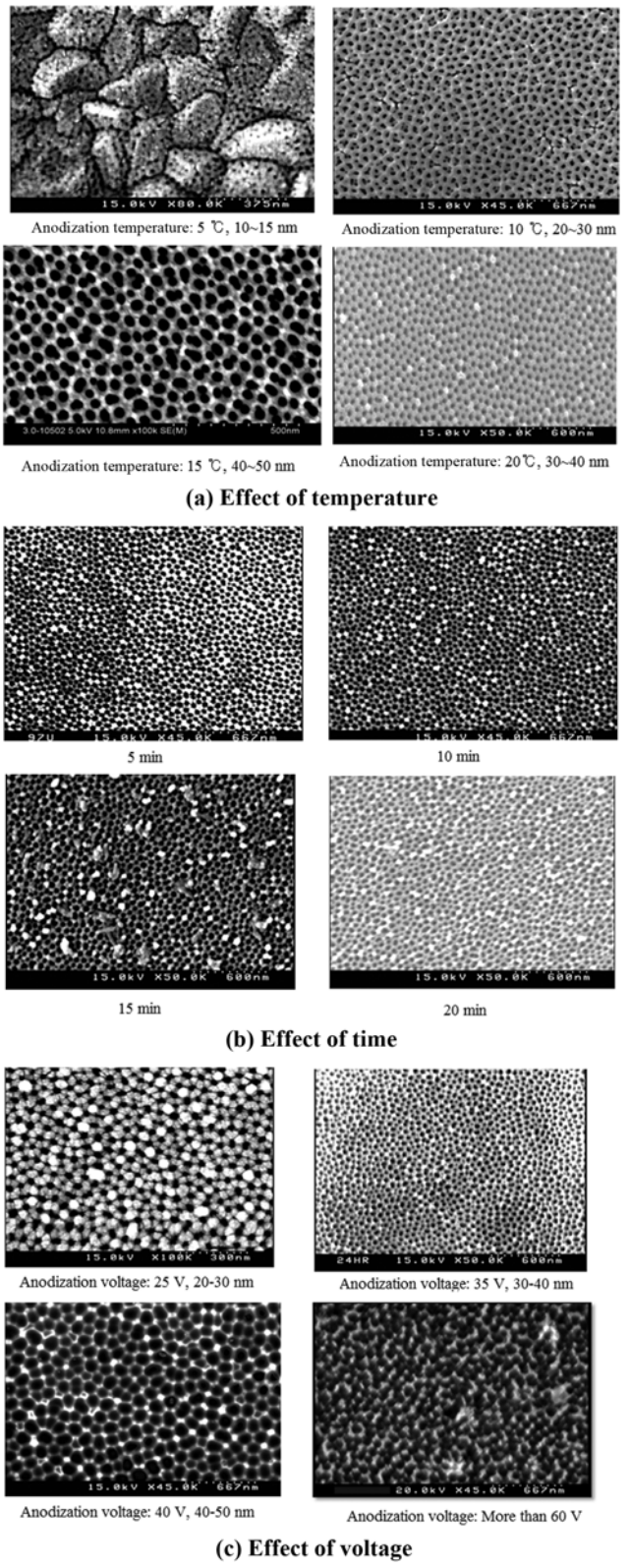

Fig. 5. Effect of experimental parameters (voltage, temperature and treatment time) on nanopore arrays.

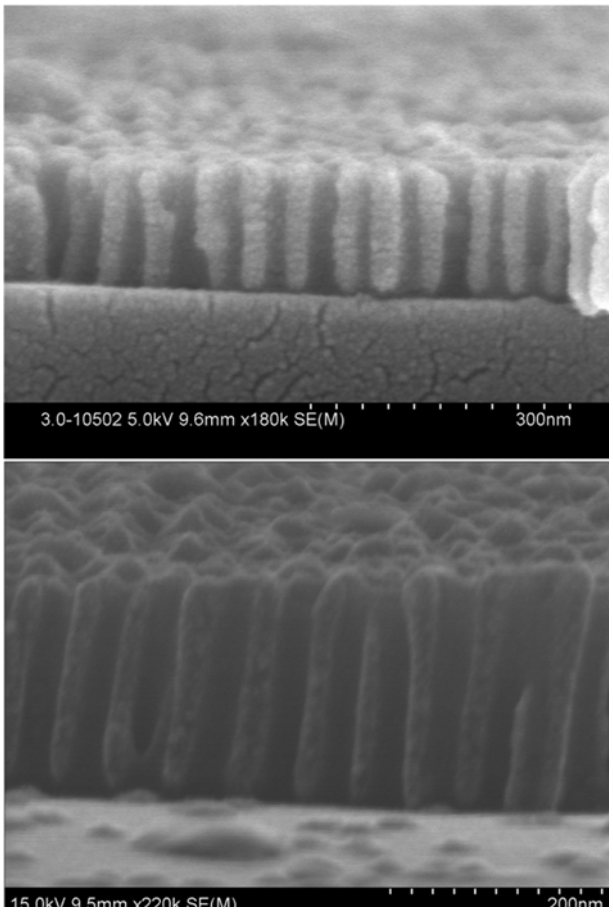

Fig. 6. Cross-sectional view of SEM image of AAO/Si template.

Table 2. Experimental conditions of pore forming process at various temperatures

Voltage	1st Anodization	Etching (0 V, 65 °C)	2nd Anodization
25 V	3 min (5 °C)	10 min	3 min (0 °C)
25 V	3 min (10 °C)	10 min	3 min (5 °C)
25 V	3 min (15 °C)	10 min	3 min (10 °C)
25 V	3 min (20 °C)	10 min	3 min (15 °C)

endothermic. The excessive heat not only triggers burning or breakdown of an anodic film but also promotes undesired acidic dissolution of the oxide membrane by the electrolyte. From the literature, it is reported that the temperature increase favors the dissolution of alumina and increases the pore diameter (from 18 to 48 nm) [15].

2-1-2. Effect of Anodizing Time on Pore Diameter

Fig. 5(b) shows that with increasing time, the pore size increases, but the pore density decreases: The pore increases in size by merging with adjacent pores. The pore density is initially high but decreases with anodizing time as dominant pores deepen [19]. Table 3 shows the detailed experimental conditions to monitor the influence of anodizing time on pore diameter. Pore growth may be due to a field-assisted hydrogen ion attack on the oxide layer. From the results, one can observe that the pore depth increases with increase of anodizing time from 5 min (pore depth; 130 nm) to 15 min (pore depth; 290 nm). With further increase in anodizing time, the pore depth decreased to 139 nm.

Table 3. Experimental conditions of pore forming process at various treatment time

1st Anodization (25 V)	Etching (0 V, 65 °C)	2nd Anodization (25 V)
3 min (15 °C)	5 min	5 min (15 °C)
3 min (15 °C)	5 min	10 min (15 °C)
3 min (15 °C)	5 min	15 min (15 °C)
3 min (15 °C)	5 min	20 min (15 °C)

Table 4. Experimental conditions of pore forming process at various voltages

Voltage	1st Anodization	Etching (0 V, 65 °C)	2nd Anodization
25 V	3 min (15 °C)	5 min	5 min (15 °C)
35 V	3 min (15 °C)	5 min	5 min (15 °C)
40 V	3 min (15 °C)	5 min	5 min (15 °C)
60 V	3 min (15 °C)	5 min	5 min (15 °C)

2-1-3. Effect of Anodizing Voltage on Pore Diameter

To investigate the effect of voltage on pore diameter (Fig. 5(c)) at constant time (5 min) and temperature (15 °C), a range of voltages (25 V, 35 V, 40 V, and more than 60 V) was selected, and the changes in the pore diameter variation were monitored. From the SEM analysis shown in Fig. 5, it is clear that the voltage has predominant effect on uniform pore formation. Pore diameters of ~20-30 nm, ~30-40 nm and ~40-50 nm were formed in the template for the applied voltage of 40 V, 50 V and 60 V, respectively. But at 60 V or above, the pores are almost collapsed. This trend is also supported elsewhere [20], and Table 4 shows the experimental conditions which were adopted to investigate the effect of voltage on nanopore diameter.

From the above-mentioned observations, one can conclude that too high voltage will lead to the destruction of the pores, which occurred at or above 60 V in this study. This trend is also supported by earlier research, where they used 40 V for pore formation [19]. The potential of the process increases as the current density increases, and therefore the pore density decreases [21-23], resulting in a lower pore density and a bigger cell size.

2-2. Electrodeposition of Cu in AAO/Si Template

Direct electrochemical deposition of Cu films on planar electrodes is a well known procedure. The deposition of Cu into the pores of anodic oxide films is complicated by side reactions involving the anodic oxide such as reanodization, dissolution, and Al_2O_3 corrosion, which can even result in the destruction of the porous film. Attempts to use the conventional aqueous acid electrolytes containing Cu^{2+} to deposit Cu on an AAO/Si electrode resulted in a fairly good deposition in this study. When the time greater than the minimum deposition time, t=20-30 min, was applied across the cell, the AAO electrode developed a uniform color starting as a light sky-blue, which ultimately became a deep metallic pigment film, presumably as a result of the deposition of Cu into the AAO pores. The deposition rate and minimum deposition time were found to

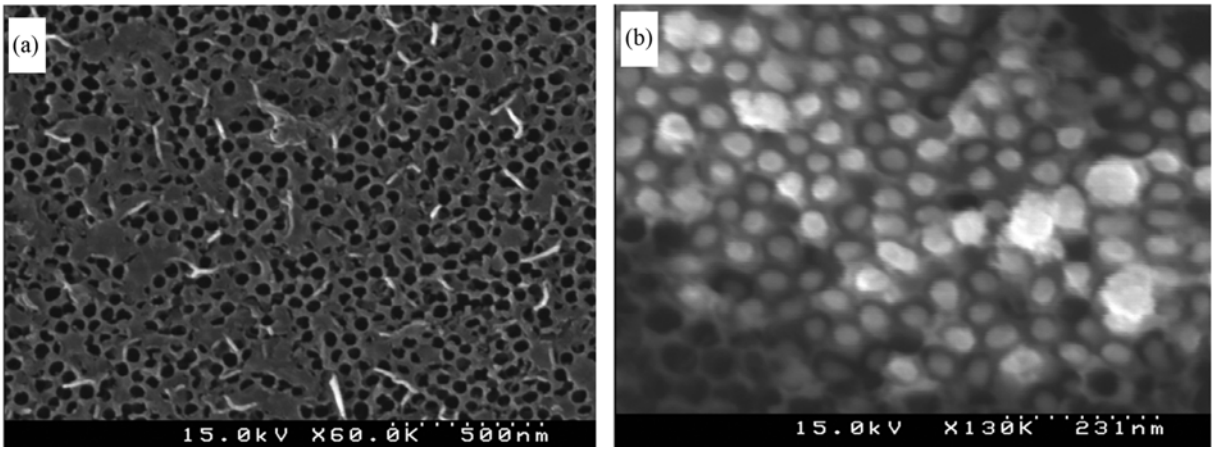

Fig. 7. SEM image of Cu nanoparticle array at various magnifications: (a) 500 nm and (b) 231 nm.

depend on the pore diameter and electrolyte temperature.

Fig. 7(a) and (b) show a SEM images of the nanopillars of Cu on the Si with or without removal of AAO template on Si surface. The Fig. 7(a) shows the nanopillars of the Cu when the AAO template has not been removed. To achieve steep side walls, it is essential that the etching process is slow enough for the etchant to penetrate deep into the pores. Both the etchant concentration and the etching time are the key factors that determine the profile of the nanoporous structures. So, the nanopillars of Cu were not that much clear in the microscopic image. Fig. 7(b) shows the nanopillars after the AAO template has been partially removed. Now it is clear that the diameter and the periodicity of the Cu-nano pillars have been directly transferred from the AAO template. An almost spherical shape configuration of copper nanopillars is observed. One of the numerous advantages of this material is the ability to control its pillar width and pillar length over wide size ranges from a few up to several hundred nm with the adjustment of the size of the AAO template by varying its experimental conditions. The width depends directly on the anodization voltage and the length on the anodization time.

As can be also seen from Fig. 7(b), the Cu nano-pillars grow upward from template bottom and have strong orientation quality. The diameter of the Cu nano-pillar is 30-40 nm, correlating well with

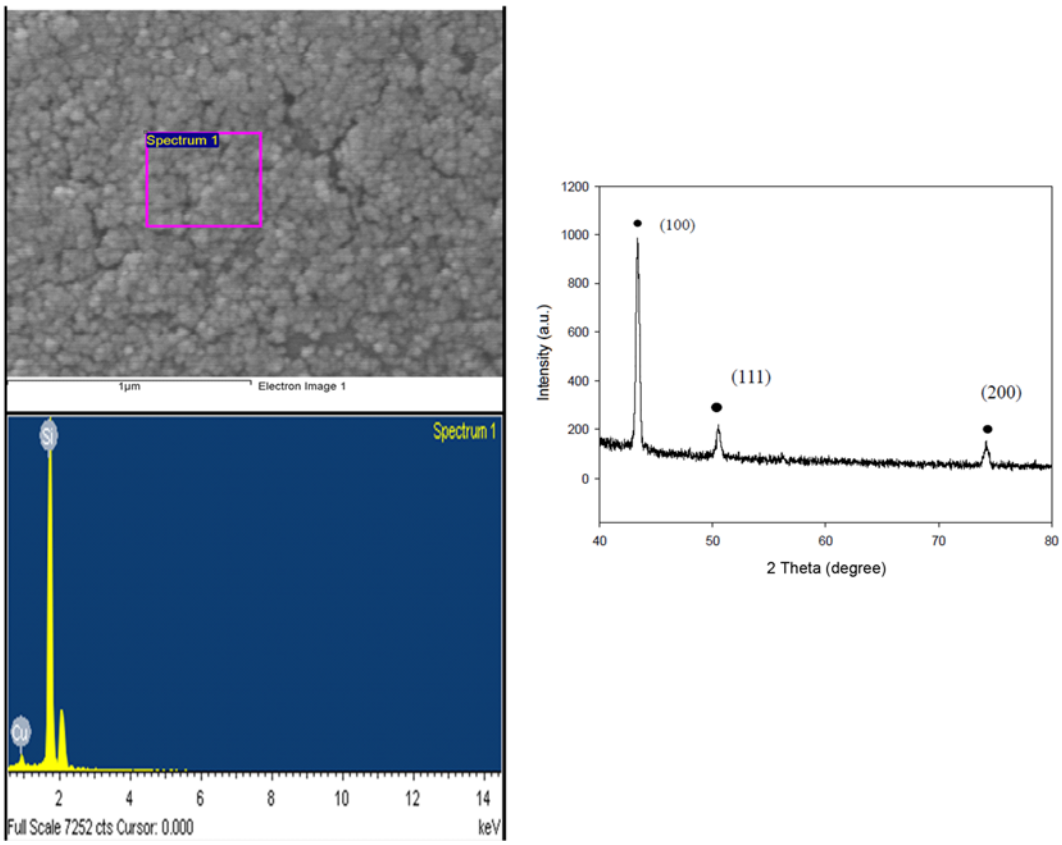

Fig. 8. Elemental (EDS) and phase compositional (XRD) analysis of copper deposited AAO/Si template.

the nanopore diameters of the AAO template formed from aluminum sputtering on Si. Aspect ratio (the ratio of length to diameter) of Cu nanopillars which are determined by the original AAO template can be adjusted accurately by controlling the thickness and pore diameter of the template. The average diameters of the copper nanoparticles and copper nanowires were reported to be 26-63 nm [24] and 10 nm [25], respectively, by earlier researchers. It is well established that Si acts as an effective mask material in Cu electrodeposition process.

3. Phase and Elemental Analysis

Fig. 8 shows the X-ray diffraction pattern of the electrodeposited Cu in porous alumina. A large peak corresponding to alumina and several minor peaks corresponding to a variety of Cu planes are seen. Peaks at 2θ positions of 44°, 52° and 74° correspond to the planes (100), (111), (200) of Cu, respectively. The presence of such a large number of Cu phases is attributed to the fact that this Cu sample was as-deposited. This is also supported elsewhere [24,26]. The oxide species of Cu are not found, indicating that the prepared copper nano-pillar is in pure metallic phase. At the same time, there is no peak related with FCC (face centered cubic) structure of routine blocks material, just the peak of HCP structure of Cu, which is attributed to the constraint of copper atoms in diameter direction caused by the forms of nanoholes during crystallization. The electrodeposition behavior of copper ions in the holes is very complicated, because the reduction of copper ions only takes place in the negative phase of sinusoidal wave during AC electrodeposition. In our case, the Cu nanopillars deposited in the AAO are estimated. All elemental signals appeared in energy-dispersive X-ray spectroscopy (EDS) shown in Fig. 8.

CONCLUSIONS

The AAO/Si template with arranged copper nano-pillar encapsulation has been investigated in this report. The template technique and structure obtained in this study have unique and promising properties for electrochemical deposition and Si-based nanodevice fabrication. The nanostructures of this study are compatible with conventional Si planar techniques and hence can be used to fabricate Si-based nanoscaled optoelectronic devices such as LEDs and solar cells. Using the AAO/Si template combined with DC electrodeposition, we have improved the process of preparing transparent Cu nano-pillars using AAO template. SEM and XRD analyses of the samples revealed the presence of Cu nanopillars in the pores of the template. It proves that the chemical electrodeposition is an effective technique to grow one-dimensional Cu nanopillars into the AAO/Si template. This technique, to a great extent, makes a good use of the electrochemical deposition method for depositing those materials whose relative salt solutions are difficult to find. Furthermore, great potential applications of this technique can be anticipated, particularly in microelectronics or nanoelectronics, since it has successfully broken through the limitation of the template application of anodic porous alumina to those important semiconductors such as Si.

ACKNOWLEDGMENTS

This work was supported by the 2009 Yeungnam University research grant (209-A-251- 230), and the Human Resource Development program of Korea Institute of Energy Technology Evaluation and Planning (KETEP) grant (No. 20104010100580) funded by the Korean Ministry of Knowledge Economy.

REFERENCES

1. P. Kohli, M. Wirtz and C. R. Martin, *Electroanalysis*, **16**, 9 (2004).
2. C. T. Kresge, M. E. Leonowicz, W. J. Roth, J. C. Vartuli and J. S. Beck, *Nature*, **359**, 710 (1992).
3. H. Masuda and K. Fukuda, *Science*, **268**, 1466 (1995).
4. S. K. Hwang, S. H. Jeong, H. Y. Hwang, O. J. Lee and K. H. Lee, *Korean J. Chem. Eng.*, **19**, 467 (2002).
5. T. Y. Kim and S. H. Jeong, *Korean J. Chem. Eng.*, **25**, 609 (2008).
6. M. Jung, J. W. Choi, Y. K. Kim and B. K. Oh, *Korean Chem. Eng. Res.*, **46**, 465 (2008).
7. Y. Lee and J. Jung, *Korean Chem. Eng. Res.*, **49**, 28 (2011).
8. Y. Li, M. Zheng, L. Ma and W. Shen, *Nanotechnology*, **17**, 5105 (2006).
9. Y. Ding, Y. J. Kim and J. Erlebacher, *Adv. Mater.*, **16**, 1897 (2004).
10. J. A. Switzer, C. J. Hung, L. Y. Huang, F. Scott Miller, Y. Zhou, E. R. Raub, M. G. Shumsky and E. W. Bohannan, *J. Mater. Res.*, **13**, 909 (1998).
11. K. Faulds, R. E. Littleford, D. Graham, G. Dent and W. E. Smith, *Anal. Chem.*, **76**, 592 **(**2004).
12. S. Ono, M. Saito and H. Asoh, *Electrochem. Solid-State Lett.*, **7**, B21 (2004).
13. G. K. Singh, A. A. Golovin and I. S. Aranson, *Phys. Rev.*, B **73**, 205422 (2006).
14. H. Asoh, K. Nishio, M. Nakao, A. Yokoo, T. Tamamura and H. Masuda, *J. Vac. Sci. Technol.*, B **19**, 569 (2001).
15. Oihane Sanz, Javier Echave, Jose Antonio Odriozola and Mario Montes, *Ind. Eng. Chem. Res.*, **50**, 2117 (2011).
16. G. C. Wood and J. P. O'Sullivan, *Electrochim. Acta*, **15**, 1865 (1970).
17. S. Setoh and A. Miyata, *Sci. Pap. Inst. Phys. Chem. Res., (Jpn.)*, **17**, 189 (1932).
18. K. Ebihara, H. Takahashi and M. Nagayama, *J. Met. Finish. Jpn.*, **33**, 156 (1982).
19. Feiyue Li, Lan Zhang, Robert and M. Metzger, *Chem. Mater.*, **10**, 2470 (1998).
20. Kathrin Schwirn, Woo Lee, Reinald Hillebrand, Martin Steinhart and Kornelius Nielsch Ulrich Gösele, *ACS Nano*, **2**, 302 (2008).
21. G. Patermarakis and H. S Karayannis, *Electrochim. Acta*, **40**, 2647 (1995).
22. G. Patermarakis and N. Nicolopoulos, *J. Catal.*, **187**, 311 (1999).
23. G. Patermarakis and D. Tzouvelekis, *Electrochim. Acta*, **39**, 2419 (1994).
24. A. Johansson, T. Törndahl, L. M. Ottosson, M. Boman and J. O. Carlsson, *Mater. Sci. Eng., C.* **23**, 823 (2003).
25. Andreas Keilbach, James Moses, RalfKohn, Markus Doblinger and Thomas Bein, *Chem. Mater.*, **22**, 5430 (2010).
26. Rosalinda Inguanta and Salvatore Piazza Carmelo Sunseri, *Appl. Surf. Sci.*, **255**, 8816 (2009).